inter·noise2003

The 32nd International Congress and Exposition on Noise Control Engineering

Jeju International Convention Center, Seogwipo, Korea,

August 25-28, 2003

[N175] Development of Combined CAA-CFD Algorithm for the Efficient Simulation of Aerodynamic Noise Generation and Propagation

Cheolung Cheong, Jewook Rye and Soogab Lee

Center for Environmental Noise and Vibration Research, Seoul National University

BD 301-1214, Seoul 151-742, Korea

Email address: accu99@snu.ac.kr

ABSTRACT

The purpose of this work is to develop efficient method for the prediction of aerodynamic noise generation and propagation in low Mach number flows in which dipole source, originating from unsteady pressure fluctuation on a solid surface, is known to be more efficient than quadrupole sources. This method is based on flow noise solvers using acoustic governing equations forced with immersed dipole source terms. The dipole source terms consist of point body forces immersed on each grid point on the solid surface. Their magnitudes are set by unsteady hydrodynamic pressure data previously calculated by incompressible Computational Fluid Dynamics Techniques. For comparison, modeled quadrupole source terms are also considered. These aeroacoustic solvers combined with CFD flow solver is applied to two-dimensional cylinder flow, which generate Karman vortex streets and resultant Aeolian tones. The properties and characteristics of sound generation process on and around the cylinder and of sound propagation through the background flows are analyzed in some detail.

KEYWORDS: Computational Aeroacoustics, Wall-Bounded Sheared Flow Noise

1. INTRODUCTION

For many industrial problems originated from aerodynamic noise, computational aeroacoustics (CAA) technique, reliable and easy to apply, would be of great value to engineers and manufacturers. Recent and spectacular achievements in the understanding of

aerodynamic noise generation mechanism are based on the CAA technique using the direct calculation of the acoustic field by solving the unsteady compressible Navier-Stokes equations. However, direct computation of the aerodynamic noise radiated by a subsonic flow where dipole noise sources are more effective than quadrupole types remains difficult because of the large computing resources, the expensive cost and physical/numerical issues [1,2] inherent in CAA. These difficulties lead to alternative methods, so-called hybrid methods which is based on the concept of variable decomposition in the governing equations into a source component and an acoustic one, which leads to two separate sets of equations governing viscous flow field and acoustic disturbance field, respectively.

In this paper, the acoustic governing equations forced with source terms, is investigated with focus brought into the dipole dominant aeroacoustic phenomena, i.e. wall-bounded shear layer problem. Modeling of dipole source terms corresponding to surface unsteady pressure fluctuations is newly developed for the acoustic governing equations. Previous study [3] is focused on the noise from free shear layer and thus is not verified to the aeroacoustic problem of wall-bounded shear flow. Current method is applied to the cross flow past a circular cylinder, which generate Karman vortex streets and resultant Aeolian tones, i.e. noise from wall-bounded shear flow. The quadrupole sources terms defined by Bailly et al. [3] are also tried to the problem.

2. FUNDAMENTAL EQUATIONS

2.1 Decomposed Euler Equations with Source Terms

If the base flow is a steady mean flow, the 2-D governing equations for the residual components are written as the following form.

$$\frac{\partial \mathbf{U}}{\partial t}+\frac{\partial \mathbf{E}}{\partial x}+\frac{\partial \mathbf{F}}{\partial y}+\frac{\partial \mathbf{E}_{nl}}{\partial x}+\frac{\partial \mathbf{F}_{nl}}{\partial y}+\mathbf{H}=\mathbf{S} \tag{1}$$

where the unknown vector is **U**, the linear flux vectors **E** and **F**, and the nonlinear flux vectors $\mathbf{E}_{nl}$ and $\mathbf{F}_{nl}$ The vector **H** consists of mean flow gradient terms, which are equal to zero when mean flow is uniform. The vector **S** represents possible unsteady sources in the flow. For the efficient description of later numerical results, some terms are defined such that Nonlinear Perturbation Equations (NPE) denote the full equations of (1), Full Linearized Euler Equation (FLEE) represents Eqs. (1) without $\mathbf{F}_{nl}$ and $\mathbf{E}_{nl}$ and Simplified Linearized Euler Equations (SLEE) is defined as the Eqs. (1) without not only $\mathbf{F}_{nl}$ and $\mathbf{E}_{nl}$ but also **H**.

2.2 Models for Unsteady Sources in the Flow

First, let's introduce a function f*(x,t)* where f is negative within the control surface, positive within the surrounding fluid and f also satisfies the equations |∇f| = *1*. Gradient of given fluctuating pressure in a solid body can be recast into the following form,

$$\nabla\left(P\cdot \mathrm{H(f)}\right)=\mathrm{H(f)}\nabla P+P\nabla \mathrm{H(f)}=\mathrm{H(f)}\nabla P+P\nabla \mathrm{f}\delta(\mathrm{f}) \tag{2}$$

where H is a heaviside function, $P(\mathbf{x},t)=p(\mathbf{x},t)-p_0(\mathbf{x})$ and $p_0(\mathbf{x})=\lim_{T\to\infty}\frac{1}{T}\int_{-T}^{T}p(\mathbf{x},t)dt$

Then, in computation domain,

$$\nabla\left(P\cdot H(f)\right)=P\nabla f\delta(f)\,. \tag{3}$$

Then, the vector **S** is written as

$$\mathbf{S}=\begin{bmatrix}0 & S_1 & S_2 & 0\end{bmatrix}^T=\begin{bmatrix}0 & P\delta(\mathrm{f})\nabla \mathrm{f}_1 & P\delta(\mathrm{f})\nabla \mathrm{f}_2 & 0\end{bmatrix}^T \tag{4}$$

Data provided by incompressible or compressible simulations can be used to estimate S_i. Quadrupole source model (QSM) by Baily et al. [3] is also considered, which is defined as

$$S_i=-\left(\partial\rho U_iU_j/\partial x_j-\overline{\partial\rho U_iU_j/\partial x_j}\right) \tag{5}$$

where $U_i(\mathbf{x},t)=u_i(\mathbf{x},t)-u_{i,0}(\mathbf{x})$ and $u_{i,0}(\mathbf{x})=\lim_{T\to\infty}\frac{1}{T}\int_{-T}^{T}u_i(\mathbf{x},t)dt$.

3.NUMERICAL METHODS

3.1 Numerical Methods for Computational Aeroacoustics

All the variables are nondimesionalized with the following scales: *D* for the length scale, c_∞ for the velocity scale, D/c_∞ for the time scale, ρ_∞ for the density scale and $\rho_\infty c_\infty^2$ for the pressure scale, where c_∞ is the ambient speed of sound. The 7-point stencil, Grid-Optimized Dispersion-Relation-Preserving (GODRP) Scheme of Cheong & Lee [4] is utilized for the spatial flux derivations of Eq. (1). The artificial selective damping by Tam & Shen [5] is used for numerical damping terms. Time integration is performed with the low-dissipation and low-dispersion Runge-Kutta schemes by Hu et al. [6]. The other boundary conditions are formed by the linearized momentum equations and the equation of conservation of the acoustic speed, as adapted from Tam and Webb [7]. Ghost value of pressure [8] is used as the wall boundary condition.

3.2 Numerical Modeling for Immersed Surface Dipole Sources

The delta function is modeled as

$$\delta(\mathbf{x}) \cong \left(\ln 2/\pi\sigma^2\right)\exp(-\ln 2\cdot \mathbf{x}^2/\sigma^2), \tag{6}$$

Both sides of the equations satisfy the following space integral equation.

$$\int_{-\infty}^{\infty}\int_{-\infty}^{\infty}\delta(\mathbf{x})dx_1dx_2 = \int_{-\infty}^{\infty}\int_{-\infty}^{\infty}\left(\frac{\ln 2}{\pi\sigma^2}\right)\exp(-\ln 2\cdot \mathbf{x}^2/\sigma^2)dx_1dx_2 = 1 \tag{7}$$

Although Eq. (7) guarantees the conservation of total energy of the delta function, there is still difference in the distribution of source energy of (6). It is evident that, as the value of σ is decreased, modeling Eq. (6) becomes more close approximation for the delta function. Combining (7) and (4), final immersed surface dipole model is numerically expressed as

$$S_i(\mathbf{x},t) = P(\mathbf{x},t)\cdot\left(\frac{\ln 2}{\pi\sigma^2}\right)\exp(-\ln 2\cdot \mathrm{f}(\mathbf{x},t)^2/\sigma^2)\nabla \mathrm{f}_i(\mathbf{x},t) \tag{8}$$

4. NUMERICAL RESULTS

The Reynolds number based on the cylinder diameter is equal to 1.58×10^4. The circular cylinder diameter and the uniform upstream velocity are *9.55 mm*, and *24.5 m/s*, respectively. The choice of these conditions is due to the existence of experimental data for the validation of flow simulations.

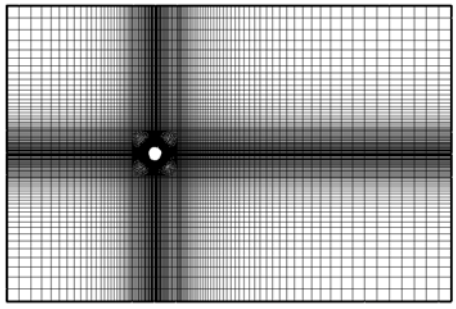

Fig. 1 The computational mesh

4.1 Numerical Results of Viscous Flow Simulation

The numerical method used for viscous flow simulation is based on the unstructured grid finite volume method, which has been described in detail by Kang et al. [9]. The computational domain used is $-10D \le x \le 20D$ and $-10D \le y \le 10D$. The flow calculations are carried out on a mesh with approximately *20000* points in the computational domain. Picture of the mesh is shown in Fig. 1. Time-dependent signals of lift and drag coefficients are presented in Fig. 2. Lift and drag coefficients show a sinusoidal variation corresponding to a Strouhal number of 0.192 and 0.384, respectively. It is expressed

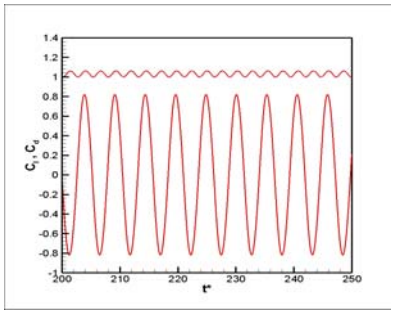

Fig. 2

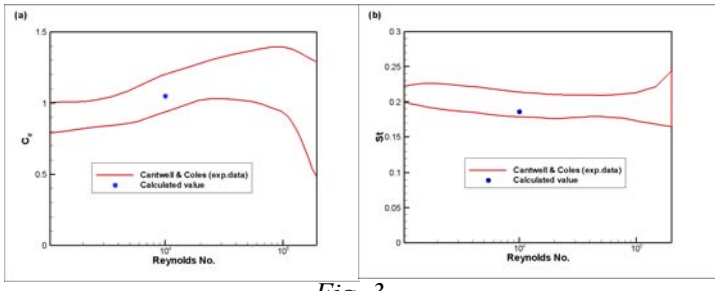

Fig. 3

that the drag should vary at twice the Strouhal number corresponding to lift. Fig. 3 shows the comparison of the average drag coefficient and vortex-shedding strouhal number with experimental data. Calculated data shows reliable agreements with experimental data.

4.2 Transformation of Flow Data for CAA Solver

Hydrodynamic unsteady data provided by the previously calculated viscous flow simulation using incompressible RANS are now used to build up the source terms of Eqs. (4), (8) and (5). Fig. 4 shows fluctuating pressure $P - p_0$ on the cylinder surface at one quarter of a cycle, at a half cycle, at three quarters of a cycle and at the beginning of a cycle, respectively. The quadrupole source terms of Eq. (5) are also obtained from the flow velocity data transformed into the grid and time domains of acoustic simulation from the grid and time domains of viscous flow simulation. The resultant terms are shown in Fig. 5. It can be found that the source term S_1 have half period as that of the source term S_2. Quadrupole source terms are calculated in a near-field domain of size [*(-10D, 20D), (-10D, 10D)*], which is large enough to avoid significant truncation of the source terms. However, Dipole source data is stored in only 5.7 Megabyte file while quadrupole source data of Eq. (5) in 1676.7 Megabyte file.

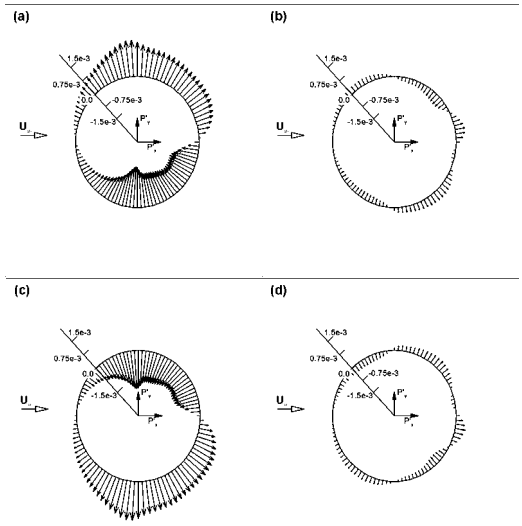

Fig. 4

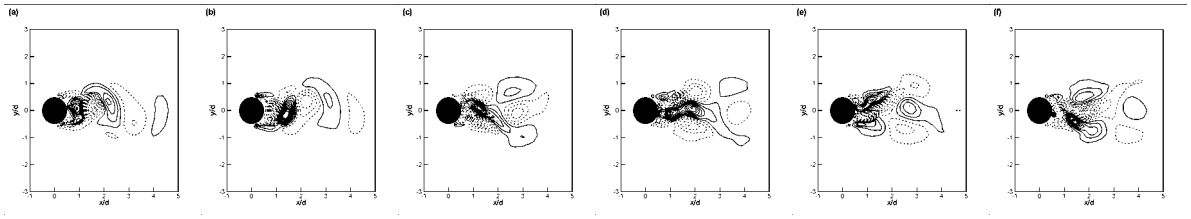

Fig. 5 Representation of quadrupole source terms; —, positive values and ---, negative values : (a) and (b) show normalized S_1 *. (c), (d), (e) and (f) show normalized* S_2

4.3 Numerical Results of CAA Solver

4.3.1 Acoustic results without mean flow effects

In Fig. 6, fluctuating pressure field obtained from the simulation using the ISDM in ambient condition is plotted at nondimensional time instant $T = 250$. As

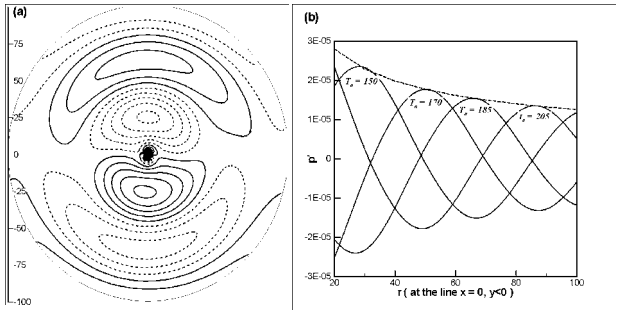

Fig. 6

expected, the acoustic wave is mainly propagated in the direction normal to the freestream velocity. Fig. 6b shows the pressure waveform along the y-axis ($y < 0$) at various times. These waveforms conform to the *2-D* wave propagation characteristics, i.e. decaying proportional to $r^{-0.5}$. The time history of the fluctuating pressure, measured at a distance $r = 99D$ from the cylinder center, is shown in Fig. 7 at four circumferential positions. It is found that the pressure signals at $\theta = 90°$ and 270° are dominated by the strouhal frequency and the signals at 0° and 180° by twice the strouhal frequency. This is physically correct result because the lift dipole is dominant at the strouhal frequency and the drag dipole at twice the strouhal frequency. The directivity pattern of the current simulation using the ISDM without mean flow, measured at a distance $r = 99D$ from the cylinder center, is shown in Fig. 8. Numerical result shows good agreement with analytic solution.

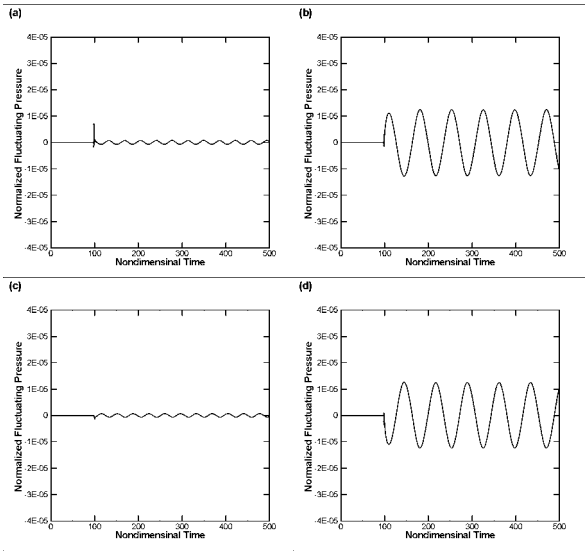

Fig. 7 (a) θ = 0°, (b)90°, (c) 180°, (d) 270°

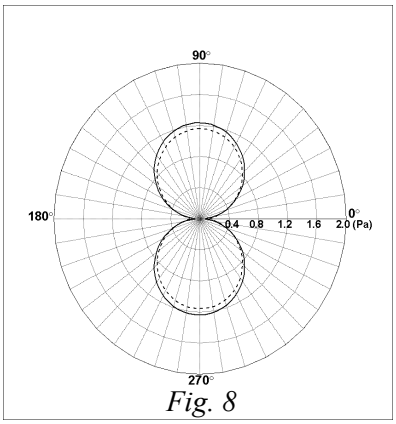

Fig. 8

Numerical simulations are also carried out with the QSM without mean flow effects. Fig. 9 shows fluctuating pressure field obtained from the QSM in ambient condition. Propagation patterns of acoustic wave are quite different from those from the ISDM. Dipole patterns in the flow direction are dominant. Magnified plot of Fig. 9b shows that the S_1 source of Eq. (8) dominates the S_2 source of Eq. (8) in the near field. However, they are physically unrealistic.

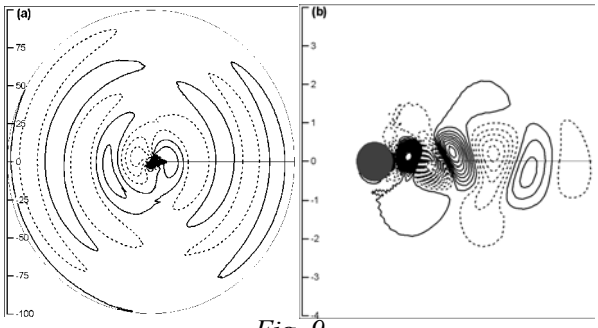

Fig. 9

4.3.2 Acoustic Results with LEE

Fig. 10 shows the directivity patterns of the ISDM connected with the SLEE. Directivity patterns from this model show results similar to those from the ISDM without mean flow effects. But, due to the Doppler effects of mean flow, directivity envelope is slightly inclined toward the upstream. Directivity envelope of numerical result is smaller than that of analytic

result. This discrepancy is related to the energy transfer from acoustic wave to vorticity wave on the solid wall. Fig. 11 shows vorticity contours around a cylinder at each time. These vortices are generated by the immersed surface dipole sources and solid boundary condition. Real physical noise generation mechanism related to the noise from a cylinder can be understood as the transformation of the energy of vorticity waves into acoustical energy. Because the immersed surface dipoles model the resultant acoustic dipole sources without describing the origin of acoustic energy, unphysical phenomena appear in the numerical simulations. However, the main concern of the acoustic simulation is the propagating acoustic wave. The ISDM provides sufficient information for the purpose only if some corrections are made to the amplitude of the original ISDM, which compensates the loss of the original acoustic energy. However, general correction factor, applied to the general problems, remains to be achieved. Fig. 12 presents the pressure fields from the QSM with the SLEE and the FLEE at certain times. The directivity patterns of the QSM with the SLEE show the omni-directional monopole-type patterns while those of the QSM with the FLEE lift-dipole patterns. From these facts, it is found that the **H** terms play a crucial role in the acoustic wave propagation from a cylinder. However, the numerical solutions of the QSM and the ISDM linked with the FLEE seem to suffer from the unstable solutions as mentioned by Bogey et al. [3].

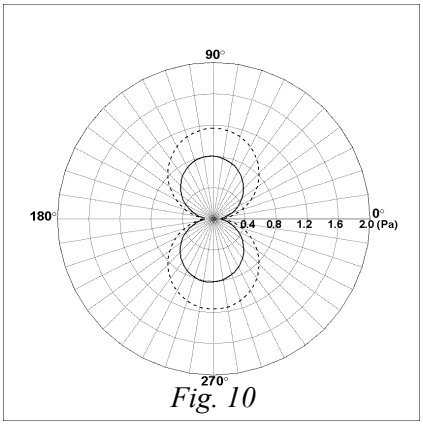

Fig. 10

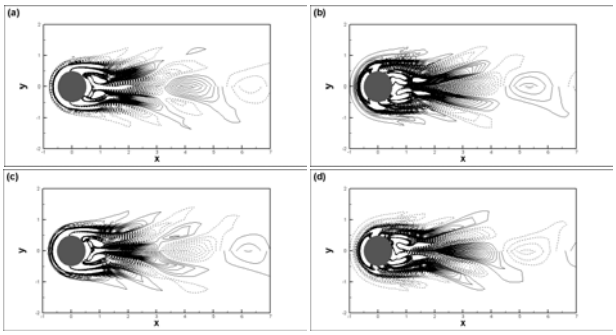

Fig. 11

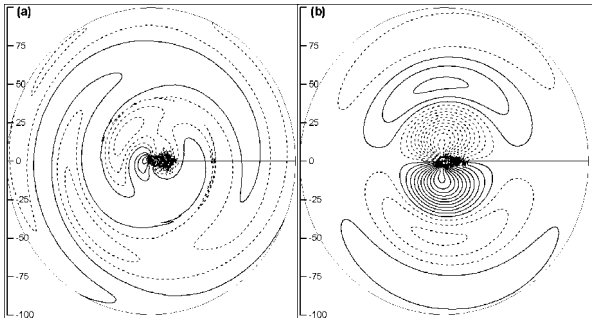

Fig. 12

4.3.3 Acoustic Results with the NPE

Fig. 13 shows the time histories of the fluctuating pressure, calculated at a distance r = 99D and $\theta = 90°$ (a) by the ISDM with the NPE and (b) by the QSM with NPE. Comparing this with the results of the ISDM

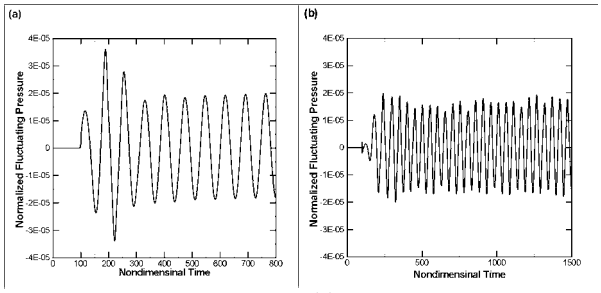

Fig. 13

with the SLEE, the magnitude of the oscillating pressure is increased. The signals of (b) seem to be dominated by the Strouhal frequency but low frequency components about 4~6 times lower than the Strouhal frequency coexist. They attributed the origin of low-frequency components to a combination of non-uniformly located sources and refraction of the dominant acoustic wave by the cylinder. This statement seems to be partially true because the signals from the ISDM with the NPE do not show such low frequency components. Through the comparison of these results, it is found that the low frequency components are related to the interactions of non-uniformly located sources and nonlinear interaction terms of Eq. (1). It is also found that the nonlinear interaction terms suppress the unstable waves which exist in the previous calculation using the FLEE.

CONCLUSIONS

For a hybrid method the immersed surface dipole model (ISDM) is developed for the efficient computation of aerodynamic noise in low Mach number flow. The immersed surface dipoles are synthesized based on hydrodynamic pressure fluctuations on solid surfaces, which are calculated by incompressible aerodynamic simulations. The ISDM combined with various acoustic equations such as simplified linearized Euler equations (SLEE), Full linearized Euler equations (FLEE) and nonlinear perturbation equations (NPE) are applied to the simulation of aeolian tone noise from a cylinder in cross flow. For comparison, the modeled quadrupole sources combined with the acoustic equations are also considered. The numerical result using the ISDM without background flow shows a convincing agreement with the analytic result. Based on this result, the ISDM without background flow is recommended for very small Mach number flow, i.e., in the limit $M \to 0$.

REFERENCES

1. C.K.W. Tam, "Computational Aeroacoustics: Issues and Methods", AIAA 95-0677 (1995)
2. S.K. Lele, Computational Aeroacoustics: A Review. AIAA 97-0018 (1997)
3. C. Bogey, C. Bailly, D. Juve, "Computation of flow noise using source terms in linearized Euler's equations", AIAA Journal **40** 235-243 (2002)
4. C. Cheong and S. Lee, "Grid-Optimized Dispersion-Relation-Preserving Schemes on General Geometries for Computational Aeroacoustics", Journal of Computational Physics **174** 248-276 (2001)
5. C.K.W. Tam and H. Shen, "Direct computation on nonlinear acoustic pulses using high-order finite difference schemes", AIAA paper 93-4325 (1993)
6. F.Q. Hu, M.Y. Hussaini, J.L. Manthey, "Low-dissipation and low-disperion Runge-Kutta schemes for computational aeroacoustics", Journal of Computational Physics **124** 177-191 (1996)
7. C.K.W. Tam, J.C. Web, "Dispersion-relation-preserving schemes for computational acoustics", Journal of Computational Physics **107** 262-281 (1993)
8. C.K.W. Tam, Z. Dong, "Wall boundary conditions for high-order finite difference schemes for computational aeroacoustics", Theoretical and Computational Fluid Dynamics **8** 303-322 (1994)
9. D.J. Kang, S.S. Bae, S.W. Joo, "An Unstructured FVM for the Numerical Prediction of Incompressible Viscous Flows", *Transactions of the KSME* **22** 1410-1421 (1998)